17th Australasian Fluid Mechanics Conference
Auckland, New Zealand
5-9 December 2010

Bottom boundary layer dynamics in an internal wave generation zone

C.E. Bluteau[1,2], N.L. Jones[1,2], G.N. Ivey[1,2], C.B. Pattiaratchi[1,2]
[1]School of Environmental Systems Engineering & [2]The UWA Oceans Institute
The University of Western Australia, Western Australia 6009, Australia

Abstract

We conducted a field experiment on the Australian North West Shelf (NWS) to document mean and turbulent properties in the bottom boundary layer (BBL) at an internal wave generation site. We measured currents at 4 and temperature at 29 discrete depths over the bottom 30 m at the 400 m depth contour. Our measurements showed nonlinear baroclinic motions in the BBL with characteristics similar to internal bores or boluses propagating onshore. At spring tide, the passage of these structures was associated with high levels of energy at the buoyancy and lower frequencies and strong localised mixing was observed in the BBL. During neap tide, the colder water associated with these features appeared to be advected back to the measurement site.

Introduction

The interaction of the barotropic tide with the continental slope can generate a variety of baroclinic responses. One of the most important responses is the generation of internal waves at tidal frequencies (i.e., internal tides), which can subsequently propagate and dissipate energy over large domains and are thus considered key elements for closing the global ocean energy budget (e.g., [12]). Other types of localised baroclinic responses include internal bores and boluses in the near-boundary region [10]. Such baroclinic structures can transport colder (denser) water onshore, and can produce significant shear and intensified currents near the seabed. The type of baroclinic response generated depends on the strength of the tidal forcing (i.e., frequency and amplitude); the local vertical and horizontal density gradients; and the height and slope of the continental shelf [11]. The criticality of the slope, defined as the ratio of the topographical slope β to the wave characteristic slope α, also influences the type of response.

Critical locations, where $\alpha \approx \beta$, typically generate internal tides most efficiently [1, 5]. When the tidal forcing is very strong, laboratory experiments have shown that significant mixing and turbulence is present in the BBL, accompanied by relatively weak generation of the internal tide [5]. Under these conditions, little energy is transported away from the generation site into the interior in the form of internal waves [5]. A variety of processes can occur in the BBL at internal wave generation regions; an understanding and description of these processes is essential to the development and implementation of numerical models of the shelf regions with strong tidal forcing (e.g., [9]).

To better understand the BBL dynamics, we undertook field observations on the Australian NWS where the slope was critical. We observed a variety of baroclinic responses over the 21-day experiment. Although the dynamics in the BBL depended on the strength of the steady tidal forcing, the observations often revealed unsteady, transient motions in the BBL.

Methods

Study site

Internal waves are frequently observed on the Australian NWS during the summer months when the water column is temperature stratified. Near the North Rankin platform (NRA), nonlinear internal waves (e.g., solitary wave packets) are regularly observed as the offshore-generated waves enter shallower water [4, 9]. Based on previous field monitoring programmes conducted by the oil and gas industry and numerical modelling results from the Regional Ocean Modeling System [8, 9], we identified a likely internal wave generation location for our field site, 65 km from NRA in 400 m of water (figure 1).

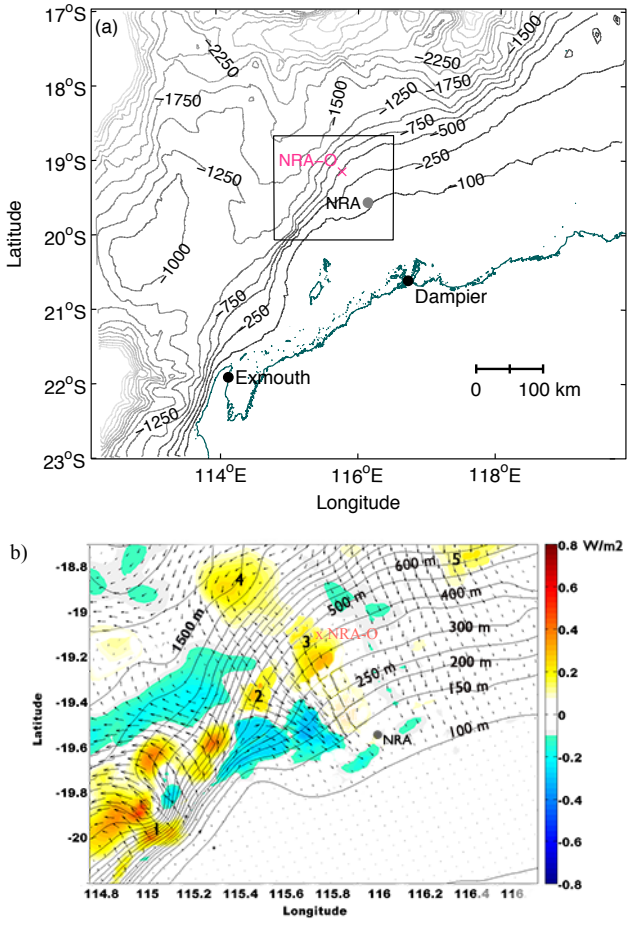

Figure 1: a) Bathymetric map of the Australian NWS with the inset b) showing the local bathymetry; the baroclinic energy flux (vectors); and the divergence of the baroclinic energy flux (colour) taken from the numerical model results of [8]. NRA-O refers to the location of our 30 m long mooring and NRA refers to the North Rankin platform.

The M_2 semi-diurnal lunar constituent, followed by diurnal constituents, dominates the tidal forcing in the region (figure 2). The topographical slope at this site is aligned at a bearing of 127° from true north (figure 1). The slope is near critical (i.e., $\alpha \approx \beta$) and the major axis of the barotropic tidal ellipses is oriented in the cross-shore direction around the 400 m bathymetry contour [4, 9]. The cross-shore alignment of the barotropic ellipses is ideal for generating baroclinic motions as this forces large excursions of stratified water up- and down-slope [1]. Spatial maps of the baroclinic energy flux, estimated from the numerical modelling output for summer 2004 [8] (their buoyancy period was representative of that measured during our field experiment, 10 min), show the propagation of baroclinic energy through the region during the spring (figure 1b) and neap tides (not shown). The positive baroclinic flux divergence from the model output implies that our selected site is in a zone of baroclinic energy generation, with energy tending to propagate shoreward before ultimately dissipating in shallow water (figure 1).

Field measurements

We deployed a mooring from 24 October to 13 November 2008 over the bottom 30 m of the water column at the 400 m depth contour approximately 195 km from the coast (figure 1). We measured the 3-dimensional velocity at 1 Hz with four acoustic Doppler velocimeters (ADV, Nortek AS) located 1.7, 3.6, 14.1, 28.1 m above the seabed (ASB). The near-bottom vertical density structure was measured with 28 thermistors (SBE39, Seabird Electronics) spaced at approximately 1 m intervals from 0.4 to 29.1 m ASB. Of these thermistors, five sampled at 1 Hz, while the remainder sampled at 0.1 Hz. We measured conductivity at 16.0 m ASB (SBE37, Seabird Electronics). Three of the ADVs also measured pressure at 1 Hz; their sampling volume was located at 3.7, 14.2, and 29.3 m ASB. During our deployment, we observed very little movement of the mooring. The mooring remained taut throughout the deployment and the maximum vertical displacement of the top-most thermistor was less than 10 cm. The memory card of the ADV located at 28.1 m ASB was faulty, resulting in the loss of 9.6 days of data, predominantly during the spring tide.

Results & Discussion

Background conditions

During the field experiment, stratification in the bottom 30 m was dominated by temperature rather than by salinity. The full-depth density profiles obtained during the mooring deployment and retrieval were very similar and showed that the water column was nearly linearly stratified, although stratification weakened near the bottom, especially below 250 m. Over the bottom 30 m, the background buoyancy frequency N=1×10^{-2} rad s^{-1} (i.e., a buoyancy period of 10 min) was estimated from the time-averaged density profile computed from the 29 temperature readings and the measured salinity at 16.0 m ASB. Observed temperature over the bottom 30 m varied from 9.58 to 12.74°C over the deployment.

Temperature spectra revealed that for all 29 thermistors, significant peaks (above the 95% confidence level) were observed at the semi-diurnal and diurnal frequencies (not shown). Although, there was evidence of a secondary peak at the Coriolis frequency f (4.76×10^{-5} rad s^{-1}), the total length of our records was too short to completely separate f from the diurnal frequency at this latitude. Between the semidiurnal forcing frequency and N, the energy decreased monotonically with distance from the seabed. At frequencies greater than N, the turbulent portion of the spectrum, more energy was contained in the measurements between 7.0 and 11 m ASB than elsewhere in the bottom 30 m of the water column.

The mean velocity magnitude encountered during the deployment was 0.10, 0.12, 0.13, and 0.13 ms^{-1} at 1.7, 3.6, 14.1, 28.1 m ASB, respectively. The apparent similarity in time-averaged velocities in the upper two instruments was due to a gap in the data over the spring tide for the ADV at 28.1 m ASB. Velocities in the BBL peaked at 0.42 ms^{-1} at 14.1 m ASB. Strong currents (>0.30 ms^{-1}) were not confined to the spring tides: the time-averaged horizontal velocities during the neap cycle were no different than those computed over the entire record. We also observed strong velocities near the seabed during the ebb phase of the tide.

The measured velocities cannot be explained by the oscillatory forcing of the surface tide alone, although horizontal velocity spectra revealed significant peaks above the 95% confidence level at the semidiurnal and diurnal frequencies (not shown). The major axes of our observed velocity tidal ellipses were oriented cross-isobath, but were more circular than that of the surface tide (not shown). Principal component analysis showed that at 1.7 and 3.6 m ASB, water generally flowed cross-isobath i.e., up- and down-slope. Higher in the water column more frequent periods of along-isobath flow were observed. These features suggest the presence of a baroclinic signal in the velocity observations.

The vertical temperature structure often deviated from the time-averaged temperature profile. Vertical stratification tended to increase during the ebb phase and decrease during the flood phase. However, sudden nonlinear displacements of the isotherms were frequently observed, generally just before high tide during the spring tides. These isotherm responses were associated with the rapid advection of cold water up-slope, especially close to the bed. During the subsequent ebb, the cold water often persisted or was advected back to our measuring site; this was particularly true of the neap tidal cycle. Preceding the large isotherm displacements typical of the spring tide, the measured currents displayed strong vertical shear in the horizontal velocities, especially between 3.6 and 14.1 m ASB, and current intensification was observed close to the seabed at 1.7 and 3.6 m ASB. In summary, in response to the tidal forcing the observations show a varied, unsteady, and strong baroclinic response in the BBL over the entire spring-neap cycle.

Time-frequency analysis

To examine this highly unsteady response, we conducted wavelet analysis [7] of the temperature measurements to provide a time series of the spectral energy. First, the results of the wavelet analysis at specific frequency bands were depth-averaged to help identify when energetic events occurred during the spring-neap cycle (figure 2). We selected suitable frequency bands by inspection of the wavelet spectra timeseries at each depth. The wavelet analysis revealed the intermittent occurrence of significant peaks (95% confidence levels) around both the buoyancy period of 10 min and also at lower harmonics, around 20, 30-60, 60-90, 180 and 360 min (figure 2b). We then used the temperature variance contours to establish the location where frequencies close to the buoyancy frequency were energized.

While high energy at the buoyancy frequency was sometimes observed over the entire 30 m measurement height (figure 3a), this energy was generally concentrated around the location of the maxima in the local vertical temperature gradient (i.e., the 10.75-11.25 °C isotherms for the 24 h data segment shown in figure 3a). These peaks were often observed during the flood phase of the spring tide (e.g., Julian days 299.5 and 299.9) and they slightly lagged the broader peaks observed at lower frequencies (e.g., 30-60 min in figure 2). These high energy levels, at both N and lower frequencies, varied in magnitude throughout the record and were not observed during every tidal cycle (figure 2).

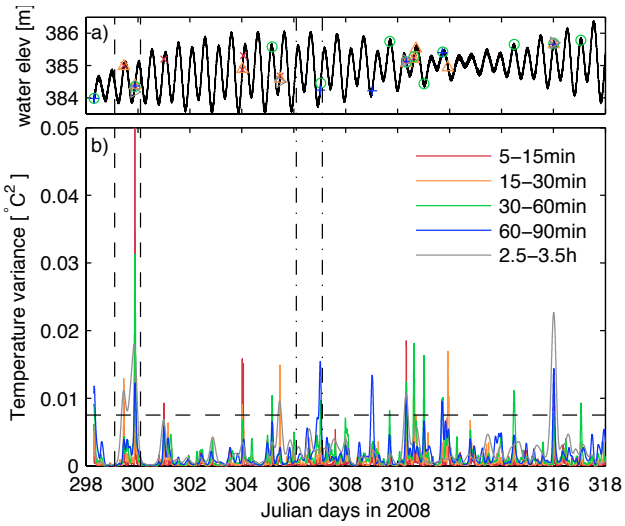

Figure 2: a) Water elevation and b) depth-averaged temperature variance for various frequency bands during the deployment. Temperature variance peaks exceeding 0.0075 $^{o}C^{2}$, the horizontal dashed line in b), are identified in a) by the coloured symbols. The 24 h period delimited by the 1st pair of vertical dashed lines is shown in figure 3 and the second pair in figure 4. For clarity, the results at 6 hours are not included.

Excitation over this range of frequencies was not simply correlated with the flood phase of spring tides. For example, the second largest depth-averaged temperature variance around the buoyancy frequency *N* occurred during ebb tide at the onset of the neap cycle around 310.3 Julian days (figure 2). This period coincided with advection of the coldest water (9.58 ^{o}C) observed during the deployment. This cold water was not confined to the ebb phase of the tide; it returned during the subsequent flood phase and then persisted into the ebb phase of the following tidal cycle (~ 311.45 d). Soon after the passage of the colder water, the largest up-slope current of 0.42 ms^{-1} was recorded at 14.1 m ASB at low tide (311.54 d). Down-slope velocities of 0.22 and 0.28 ms^{-1} at 1.7 and 3.6 m ASB, respectively, accompanied the up-slope velocity at 14.1 m ASB. This strong vertical shear in the horizontal currents preceded the subsequent peaks at lower frequencies (i.e., 30-60 and 60-90 min) in the depth-averaged temperature variance before high tide at 311.74 Julian days (figure 2). For subsequent neap-tide cycles (~311.75-314.5 d), less energy was contained at *N* and lower frequencies (figure 2).

Baroclinic events

The strongest observed depth-averaged temperature variance at the buoyancy period (299.88 d), largest horizontal velocities at 1.7 and 3.6 m ASB (299.47 and 299.35 d, respectively), and the strongest vertical velocities at 1.7 m ASB all occurred over two tidal cycles towards the beginning of the record (figure 2). These features are the result of internal bores or possibly boluses [10] passing through our measurement site during the flood phase of each tidal cycle, and from here on, we will refer to these events as internal bores.

Figure 3 covers two tidal cycles and shows successive and strong internal bores that caused isotherms to jump by as much as 20 m, accompanied by strong and highly depth-dependent velocity fields. After the tidal elevation started to increase, at 299.25 d (Fig 3a), the near-bed velocities at 1.7 and 3.6 m ASB were down-slope and strong, with peak values of 0.36 ms^{-1} at 3.6 m ASB. Further from the seabed at 14.1 m ASB, the velocities were up-slope at ~0.20 ms^{-1}, flowing almost in the opposite direction of the bottom velocities. About 5 h after low tide (299.45 d) a bore moved up-slope bringing cold deep water through the site and the isotherms jumped almost 20 m vertically in ~15 min. Following this bore, the currents reversed with near-bed velocities up-slope with peak values of 0.30 ms^{-1}, while away from the bed, currents were shifted in direction to almost due east. High energy levels at *N* over the entire 30 m subsided 50 min after the passage of the bore, and the depth-averaged values peaked earlier at 299.46 d (Figure 3a-b). During this time, vertical temperature profiles exhibited unstable overturns of several meters (not shown). Finally, 2 h after high tide at ~299.6 d, near bottom velocities were reduced to near zero and then subsequently oriented themselves down-slope as the process started to repeat over the next tidal cycle.

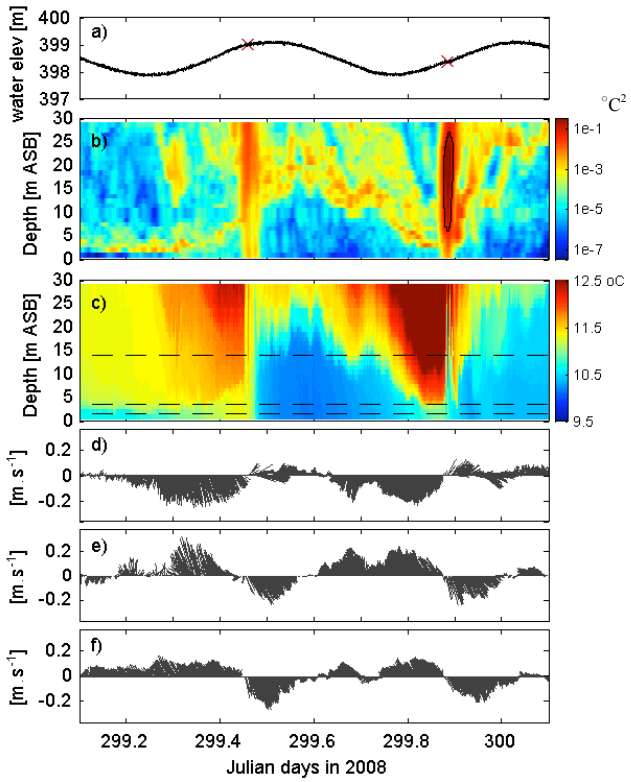

Figure 3: Baroclinic events over two tidal cycles (24 h) a) tidal elevation showing when (×) the depth-averaged temperature variance peaked at *N*; b) temperature variance around *N* (period of 5-15min) depth contour with peaks exceeding 90% confidence levels delineated by the solid black line; c) temperature contours with ADV measurement depths shown by the horizontal dashed lines; d-f) 1 min time-averaged horizontal velocities at 1.7, 3.6, and 14.1 m ASB, respectively. Note that in panels d-f, the up-slope direction is 37^{o} clockwise from the horizontal.

During this next tidal cycle, similar features were observed. Vertical shear in the horizontal velocity manifested itself during the ebb flow (after 299.65 d) between the two bottom-most ADVs and the ADV at 14.1 m ASB (figure 3d-f). The increase in energy around *N*, occurred more rapidly, approximately 2.6 h after low tide (figure 3b). Currents after the passage of the bore were weaker than during the previous event (i.e., < 0.30 ms^{-1}). After the passage of the surge at 299.88 d, the velocity at 14.1 m ASB also took longer (~100 min) to re-orient up-slope with near-bed velocities. The temperature gradient across the isotherm displacements was larger during this second event; in fact, the warm water drawn down towards the bottom prior to the bore was the warmest observed during our deployment. We estimated the internal *Fr* for the bottom layer of fluid (assuming 2-layer stratified flow) using the observed velocities and density differences observed prior to each bore to be approximately 10 and 5. Such large values are consistent with the large isotherm displacements and energetic mixing observed during these periods.

The rapid changes of energy in the various harmonics and at N for the baroclinic events shown in figure 3 suggests that these events were likely associated with strong mixing and local turbulent kinetic energy dissipation ϵ. We estimated ϵ using the inertial dissipation subrange method using 17 min (1024 samples) segments of velocity [2] (figure 4a). We then computed the vertical eddy diffusivity K_ρ, a parameter commonly used in numerical models to estimate turbulent mixing, with the method proposed by Osborn [6] (figure 4a). This method assumes a local balance of turbulent kinetic energy between shear production, buoyancy loss, and ϵ:

$$K_\rho = \Gamma \frac{\varepsilon}{N^2}, \qquad (1)$$

We assumed the upper bound for mixing efficiency of $\Gamma = 0.2$ and used our background N=1×10^{-2} rad s^{-1}. Even over a relatively quiescent period, eddy diffusivities were large and K_ρ varied from 1.3×10^{-4} to 1.0×10^{-3} m^2 s^{-1}, while ϵ =6.7×10^{-8} to 5.0×10^{-7} W kg^{-1} at 1.7 m ASB (figure 4a). We also calculated the Ellison length scale $L_e = T'/(\partial \overline{T}/\partial z)$ [3], a measure of the largest turbulent eddies in the flow, from individual temperature time series at three discrete depths over the same period as ϵ (figure 4b). Away from the bed at 7.0 m ASB, higher L_e were obtained; the mean L_e=0.27, 0.31 and 1.06 m at 0.4, 1.6, and 7.0 m ASB, respectively (figure 4b). The higher L_e estimated between 306.6 and 306.9 Julian days, especially at 0.4 and 1.6 m ASB, were during a period when horizontal velocities peaked at 0.22, 0.24, and 0.30 ms^{-1} at 1.7, 3,6, and 14.1 m ASB (not shown). At other times, horizontal velocities varied from ~0 to 0.15 ms^{-1}. To put this in context, we estimated the steady state turbulent BBL thickness as $\delta \approx \sqrt{K_\rho / \omega}$, using the semidiurnal constituent as our dominant tidal frequency. This calculation yields δ≈1-3 m, which is comparable to our observed mixing scales close to the bed. Overall, our BBL flow was highly unsteady and the full description of the links between the mean and turbulent properties is the subject of future work.

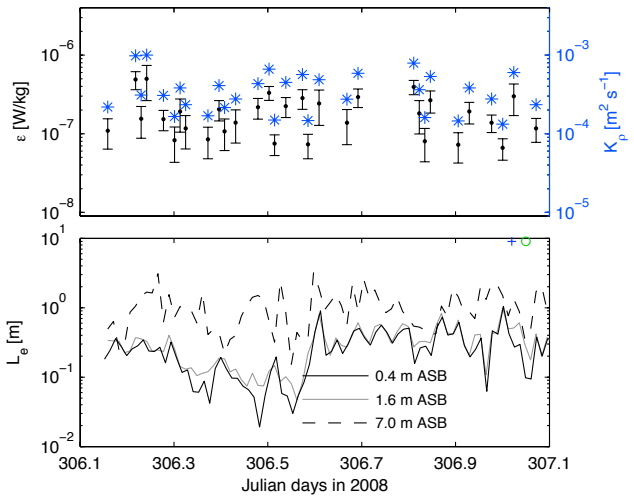

Figure 4: a) Estimated TKE dissipation ε and eddy diffusivity K_ρ at 1.7 m ASB; b) Ellison length scale L_e computed at three different depths. The symbols indicate when the depth-averaged temperature variance peaked at the 30-60 min (+) and 60-90 min (○) frequencies.

Conclusions

Our field observations in the BBL of an internal wave generation region demonstrated the transient and unsteady nature of the flow. The baroclinic features observed were more frequent during the spring tides, although the temperature records showed high energy levels at high frequencies (~N) during the onset of the neap tides. The significance of these features for mass transport on-shelf is unclear; the cold water advected up-slope during the neap events appeared to return to our site, while this return of cold water is less obvious during the spring tide baroclinic events.

Numerical models do not adequately replicate the near-bed current intensification, vertical temperature structure and the dissipation of turbulent kinetic energy observed in our field data due to a combination of lack of resolution and inadequacy of turbulent closure schemes [e.g., 8, 9]. Ongoing analysis includes comparing turbulent properties amongst baroclinic events with more quiescent periods to quantify the physical dynamics of the BBL leading towards improvements in the parameterization of these dynamics in numerical models.

Acknowledgments

This work was funded by the Western Australian Marine Science Institute (Project 6.2) and an Australian Research Council Discovery Project (DP0663334). C.E. Bluteau acknowledges the support of an International Postgraduate Research Scholarship (IPRS) and a University Postgraduate Award (UPA).

References

[1] Baines, P. G., On internal tide generation models, *Deep-Sea Res.*, **29**, 1982, 307–338.

[2] Bluteau, C. E., Jones, N. L. and Ivey, G. N., Estimating turbulent kinetic energy dissipation using the inertial subrange method in environmental flows, *Submitted to Limnol. Oceanogr.: Methods*.

[3] Ellison, T. H., Turbulent transport of heat and momentum from an infinite rough plane, *J. Fluid Mech.*, **2**, 1957, 456–466.

[4] Holloway, P. E., Chatwin, P. G. and Craig, P., Internal tide observations from the Australian North West Shelf in summer 1995, *J. Phys. Oceanogr.*, **31**, 2001, 1182–1199.

[5] Lim, K., Ivey, G. N. and Jones, N. L., Experiments on the generation of internal waves over continental shelf topography, *J. Fluid Mech.*, in press.

[6] Osborn, T. R., Estimates of the local rate of vertical diffusion from dissipation measurements, *J. Phys. Oceanogr.*, **10**, 1980, 83–89.

[7] Torrence, C. and Compo, G. P., A practical guide to wavelet analysis, *B. Am. Meteorol. Soc.*, **79**, 1998, 61–78.

[8] Van Gastel, P., *Internal wave dynamics on the Australian North West Shelf*, PhD thesis, University of Western Australia, 2010.

[9] Van Gastel, P., Ivey, G. N., Meuleners, M., Antenucci, J. P. and Fringer, O., The variability of the large-amplitude internal wave field on the Australian North West Shelf, *Cont. Shelf Res.*, **29**, 2009, 1373–1383.

[10] Venayagamoorthy, S. K. and Fringer, O. B., On the formation and propagation of nonlinear internal boluses across a shelf break, *J. Fluid Mech.*, **577**, 2007, 137–159.

[11] Vlasenko, V., Stashchuk, N. and Hutter, K., *Baroclinic Tides: Theoretical Modeling and Observational Evidence*, Cambridge University Press, 2005.

[12] Wunsch, C. and Ferrari, R., Vertical mixing, energy, and the general circulation of the oceans, *Annu. Rev. Fluid Mech.*, **36**, 2004, 281–314.